Regenerative Therapy 28 (2025) 201–213

Contents lists available at ScienceDirect

Regenerative Therapy

journal homepage: http://www.elsevier.com/locate/reth

Original Article

MAPT-A152T mutation drives neuronal hyperactivity through Fyn-NMDAR signaling in human iPSC-Derived neurons: Insights into Alzheimer's pathogenesis

Maika Itsuno [a, 1], Hirokazu Tanabe [b, 1], Etsuko Sano [a, c], Takashi Sasaki [d], Chisato Oyama [e], Hiroko Bannai [e], Koichi Saito [b], Kazuhiko Nakata [b], Setsu Endoh-Yamagami [b, ***], Hideyuki Okano [a, c, **], Sumihiro Maeda [a, *]

[a] *Department of Physiology, Keio University School of Medicine, 35 Shinanomachi, Shinjuku, Tokyo 160-8582, Japan*
[b] *FUJIFILM Corporation, Bio Science & Engineering Laboratories, 577 Ushijima, Kaisei-cho, Ashigarakami-gun, Kanagawa 258-8577, Japan*
[c] *Keio University Regenerative Medicine Research Center (KRM), 3-25-10 Tonomachi, Kawasaki-ku, Kawasaki, Kanagawa 210-0821, Japan*
[d] *Center for Supercentenarian Medical Research, Keio University School of Medicine, 35 Shinanomachi, Shinjuku, Tokyo 160-8582, Japan*
[e] *Department of Electrical Engineering and Biosciences, School of Advanced Science and Engineering, Waseda University, 2-2 Wakamatsu-cho, Shinjuku, Tokyo 162-0056, Japan*

A R T I C L E I N F O

Article history:
Received 16 October 2024
Received in revised form
29 November 2024
Accepted 11 December 2024

Keywords:
Alzheimer's disease (AD)
Induced pluripotent stem cells (iPSCs)
hTau-A152T mutation
Tau-Fyn-NMDAR pathway

A B S T R A C T

Introduction: Tau protein plays a pivotal role in the pathogenesis of Alzheimer's disease (AD) and in regulating neuronal excitability. Among tau-coding microtubule associated protein tau (*MAPT*) gene mutations, the A152T mutation is reported to increase the risk of AD and neuronal excitability in mouse models.
Methods: To investigate the effects of *MAPT* gene expression and its mutations on neuronal activity in human neurons, we employed genome editing technology to introduce the A152T or P301S mutations into induced pluripotent stem cells (iPSCs). We then differentiated them into excitatory and inhibitory neurons. As a control, iPSCs in which the *MAPT* gene was replaced with a fluorescent protein were also created.
Results: In excitatory neuronal cultures, the A152T mutation was found to enhance spontaneous neuronal activity and the association of tau and Fyn. However, in inhibitory neuron-enriched cultures, the A152T mutation did not affect neuronal activity. Inhibition of NMDA receptors (NMDAR) and the reduction of tau protein levels decreased neuronal excitability in both A152T/A152T and healthy control (WT/WT) excitatory neurons. In addition, the A152T mutation increased the interaction between tau and Fyn. These findings suggest that the tau-Fyn interaction plays a critical role in regulating neuronal activity under physiological conditions, while the A152T mutation enhances neuronal activity by strengthening this endogenous interaction between tau and Fyn. In addition, transcriptomic analysis revealed structural changes specific to excitatory neurons with the A152T mutation. Common changes observed in both A152T and P301S lines recapitulated a dedifferentiation phenotype, consistent with previous reports.
Conclusions: These data demonstrate that the A152T mutation in the *MAPT* gene increases neuronal excitability through the tau-Fyn-NMDAR pathway in excitatory neurons, shedding light on its role in AD pathogenesis.

Abbreviations: AD, Alzheimer's Disease; *MAPT*, Microtubule associated protein tau; iPSCs, Induced Pluripotent Stem Cells; NMDAR, NMDA receptor; WT, Wild Type; Aβ, Amyloid β; FTD, Frontotemporal Dementia; DLB, Dementia with Lewy Bodies; *hAPP*, human amyloid precursor protein; FTDP-17, Frontotemporal Dementia with Parkinsonism Linked to Chromosome 17; Ngn2, Neurogenin2; hTau-A152T/P301S, human Tau with the A152T/P301S mutation; DOX, Doxycycline; KO, knockout; PLA, proximity ligation assay; GO analysis, gene ontology analysis; DEGs, differentially expressed genes.

* Corresponding author.
*** Corresponding author.
** Corresponding author. Department of Physiology, Keio University School of Medicine, 35 Shinanomachi, Shinjuku, Tokyo 160-8582, Japan.
E-mail addresses: setsu.endo@fujifilm.com (S. Endoh-Yamagami), hidokano@keio.jp (H. Okano), sumihiro.maeda@keio.jp (S. Maeda).
Peer review under responsibility of the Japanese Society for Regenerative Medicine.
[1] Equally contributed.

https://doi.org/10.1016/j.reth.2024.12.009

1. Introduction

Alzheimer's disease (AD) is a form of dementia characterized by the abnormal accumulation of insoluble protein aggregates, such as Amyloid β (Aβ) peptides outside neurons and tau proteins inside neurons. Recently, there has been growing interest in the link between epilepsy and AD, as well as other related neurodegenerative diseases, within the field of neuroscience [1]. The incidence rates of epilepsy in patients with AD, frontotemporal dementia (FTD), or dementia with Lewy bodies (DLB) are higher than that in control groups [2]. In addition, the progression of cognitive impairment is faster in AD patients with epilepsy than in those without epilepsy [3]. While epilepsy could be considered merely a comorbidity with no direct interaction with AD pathogenesis, the exacerbation of epileptic symptoms and neuronal excitability is observed in several mouse models for AD-like human amyloid precursor protein (*hAPP*) overexpressing mice [4,5]. These findings indicate that epileptic symptoms in AD are not just a coexisting symptom that affects the disease progression but a driver that promotes AD pathogenesis [4]. Consistent with this idea, an anti-epileptic drug has been reported to block the impairment of some cognitive functions in AD patients [6]. The epileptic symptoms in AD model mice were blocked by tau-coding microtubule associated protein tau (*Mapt*) gene deletion, suggesting that Aβ aberrantly increases neuronal excitability in AD patients through tau [7,8]. In addition, *Mapt* over-expression exacerbated the epileptic symptoms in *hAPP* over-expressing mice, suggesting that the expression level of tau regulates the Aβ-induced epileptic condition [9].

Mutations in the *MAPT* gene cause a familial neurodegenerative disease called frontotemporal dementia with Parkinsonism linked to chromosome 17 (FTDP-17) [10]. The discovery of FTDP-17 demonstrated that tau dysfunction is enough to trigger neurodegeneration without Aβ accumulation. In addition, the *MAPT* gene mutation, in which the 152nd alanine is replaced by threonine (A152T), is a risk factor for both AD and FTD spectrum disorders [11–13], and it is the first and only *MAPT* gene mutation genetically linked to AD pathogenesis. Expression of human tau with the A152T mutation (hTau-A152T) in mice increases neuronal excitability, followed by age-dependent neuronal cell death and cognitive impairment [9]. Furthermore, neuronal cell death induced by some stressors is enhanced by the A152T *MAPT* gene mutation in induced pluripotent stem cell (iPSC)-derived neurons [14,15]. These data suggest that the A152T mutation contributes to tau pathogenesis by increasing neuronal hyperexcitability in human neurons.

Recently, neurons differentiated from the iPSCs derived from patients' cells have been utilized to elucidate molecular mechanisms caused by tau dysfunction as human neuron models that allow high throughput analysis of pathological phenotypes. For example, the A152T and R406W *MAPT* gene mutations induce neurite abnormality and enhanced vulnerability to toxic insults in iPSC-derived neuronal models [16,17]. In addition, neurons differentiated from FTDP-17 patient-derived iPSCs enhanced the intracellular Ca^{2+} response to electrical stimulation [18]. However, it is unclear how tau is involved in enhancing neuronal excitability in human neurons and whether the A152T mutation induces an epileptic effect.

To investigate the underlying mechanism, we first established isogenic human A152T iPSC lines by introducing the A152T mutation into a healthy (wild type; WT) control iPSCs using the CRISPR-Cas9 system. In parallel, we also introduced the P301S mutation, one of the most frequently used FTDP-17 mutations to study tau pathogenesis, into the healthy control iPSCs. To obtain excitatory neurons, we expressed Neurogenin2 (Ngn2) and miR-9/9*-124, a transcription factor and microRNAs that allow each iPSC cell line to directly differentiate into glutamatergic neurons, not via neural precursor cells [19]. This method enables rapid neuronal maturation of iPSC-derived neurons, enabling the measurement of neuronal excitation within two weeks. Using these iPSC-derived excitatory neurons, we examined the neural excitability and the pathogenesis caused by the A152T *MAPT* gene mutation.

2. Materials and methods

A list of Reagents and Materials is available in the supplementary material file.

2.1. Preparation of lentiviral particles for expression miR-9/9*-124

Self-inactivating (SIN) vector (CSIV-124-9/9*-mRFP-TRE-EF-BsdT) was constructed by a Multisite Gateway-based method as previously described [19]. Lentiviral particles were generated using a modified method that was previously described [19]. On day 0, HEK293T cells were passed in poly-L-Laminin-coated dishes in DMEM containing 10 % FBS, 2 mM L-glutamine, 100 U/ml penicillin, and 100 mg/ml streptomycin sulfate. The cells were cultured on 10 cm dishes at 37 °C with 5 % CO2 for 24 h. The transfection of each gene and packaging was performed using polyethylenimine. The DNA plasmids of SIN lentiviral vector (6 μg/dish), pCAG-HIVgp (3 μg/dish), pCMV-VSV-G-RSV-Rev (3 μg/dish) were mixed with 24 μl/dish of 1 mg/ml PEI in 500 μl/dish Hank's balanced salt solution (HBSS). Subsequently, the DNA/PEI mixture was mixed by vortexing and dropped onto the cells. Sixteen hours later, the medium containing the DNA/PEI mixture was changed to a fresh medium containing 10 μM forskolin to enhance viral particle production. After 48 h, the conditioned medium was collected and filtered through a 0.45 μm filter. The filtrate was concentrated by ultracentrifugation (50K x *g*, 2 h, 4 °C). After collecting the pellet containing lentiviral particles by resuspending in HBSS, the resuspension was filtered with HBSS using a centrifugal filter unit, Amicon Ultracell-100K. The titer of the lentiviral particles was measured using lenti-X GoStix Plus. The resuspension of lentivirus particles was stored at −80 °C.

2.2. Gene editing of iPSC using CRISPR-Cas9

To obtain multiple iPSC lines with the same genetic background, the iPSC line 201B7 [20] derived from a healthy person was edited at the *MAPT* gene locus (hereinafter, tau gene) encoding tau. To insert the TagGFP2 (hereinafter, GFP) gene and gene mutation into the *MAPT* gene, gene editing with targeting vectors was performed. Targeting vectors for knock-in of GFP, GFP-polyA for *MAPT* gene knockout, and A152T and P301S *MAPT* gene mutation were constructed by inserting the sequences into the HR710PA-1 vector (System Bioscience). The targeting vectors include hygromycin-resistance gene and mRFP sandwiched between left and right homology arm (LHA and RHA) and inverted terminal repeat (ITR) sequences and have hsvTK that induces cytotoxicity to gancyclovir sensitivity downstream of RHA. Therefore, cells in which the region between LHA and RHA of the targeting vector is inserted into the tau gene show hygromycin-resistant and ganciclovir-insensitive properties. Feeder-free iPSC culture was prepared as previously described [19]. Dissociated iPSCs were transfected with a targeting vector, sgRNA (Supplemental Figure Table S1), and CRISPR-Cas9 protein using the Neon Transfection System (Thermo Fisher Scientific). For the CRISPR–Cas sgRNA targets, we selected sequences that would make the editing free from the off-target using an online database tool, "CHOPCHOP" [21]. After seeding to culture dishes, iPSCs were maintained in StemFit/AK02N containing

100 μg/ml hygromycin and 2.5 μg/ml gancyclovir. After drug selection, selected iPSC colonies were harvested and amplified, and the sequence of the *MAPT* gene was confirmed. Furthermore, to remove ITR sequences which include the hygromycin-resistance gene and mRFP, the iPSC clone was transfected with excision only PiggyBac transposase expression vector using GeneJuice Transfection Reagent. Finally, six isogenic iPSCs were generated (Supplemental Table S2). WT/A152T, A152T/A152T, and P301S/P301S iPSC were obtained by knock-in of *MAPT* gene mutations to N-GFP-tau iPSC. Moreover, the P301S *MAPT* gene mutation observed in patients with FTLD-17 is the 1-base mutation from CCG to TCG, while the mutation inserted in this study is the 2-base mutation from CCG to TCC.

2.3. Establishment of iPSC lines carrying Tet-On inducible Ngn2 and miR-9/9*-124 vectors

Vectors for neuronal differentiation were transfected into the isogenic iPSC lines as previously described with minor modifications [19]. Briefly, after transfection of pCMV-HyPBase-PGK-Puro, PB-TET-PH-lox66FRT-NEUROG2, and PB-CAGrtTA3G-IH vectors, cells were maintained in StemFit/AK02N containing 50 μg/ml hygromycin and 0.5 μg/ml puromycin. Stable lines of these three vectors in 201B7, N-GFP-tau, and C-GFP-tau iPSC lines were differentiated into neurons to check neuronal induction using the procedure below. After introducing these three vectors and drug selection, miR-9/9*-124 lentivirus was added to iPSCs. After two days of lentiviral infection, the iPSC culture medium was replaced with the fresh medium containing 10 μg/mL blasticidin S, 50 μg/ml hygromycin, and 0.5 μg/ml puromycin. After the drug selection, iPSC colonies were picked and checked for neuronal differentiation using the procedure below.

2.4. Induction of purely excitatory neurons by the expression of Ngn2 and miR-9/9*124

Neuronal differentiation from iPSCs was performed as previously described with minor modifications [19]. iPSCs were dissociated using 0.5 × TrypLE Select, and 2.5 × 10^4 cells (96 well-plate) or 2.5 × 10^5 cells (12 well-plate) were seeded onto culture dishes coated with poly-L-lysine and iMatrix-511 silk into neuronal induction medium (Neurobasal Plus medium containing 2 % B27 Plus supplement, 1 % CultureOne supplement, 1 % GlutaMAX, 200 μM L-ascorbic acid, 200 μM dbcAMP, 10 μM Y27632, 20 μM DAPT and 4 μg/ml doxycycline (DOX)). On days 2–3, a half-medium change was performed with the fresh neuronal induction medium. On days 5–6, 70 % medium was changed with fresh neuronal maintenance medium (Neurobasal Plus medium containing 2 % B27 Plus supplement, 1 % CultureOne supplement, 1 % GlutaMAX, 200 μM L-ascorbic acid, 200 μM dbcAMP, and 10 ng/ml BDNF). Half-medium change was performed every 3–4 days after day 6. Day 13–22 neurons were used for all assays below. 1 μM Accell siRNA was added into culture media from day 6.

2.5. Induction of inhibitory neuron-enriched culture

We induced the inhibitory neuron-enriched culture by dual SMAD inhibition as previously reported [22]. The induced neuronal culture was maintained with BrainPhys neuronal medium (Cat: 05793, STEMCELL technologies) containing 10 ng/ml GDNF, 10 ng/ml BDNF, 200 μM ascorbic acid, 0.5 mM dbcAMP, 2 μM PD0332991 (BP + alpha neuronal medium). We confirmed that 85 % of the neurons are inhibitory and 15 % of the neurons are excitatory neurons by single-cell RNAseq (paper in submission).

2.6. Immunofluorescence

Neurons were fixed by 4 % paraformaldehyde. After washing with PBS, the neurons were incubated with a blocking buffer (5 % FBS, 0.3 % Triton-X100 in PBS). Primary antibodies (1:1000) (βIII tubulin, NeuN, MAP2, HT7, Tau-5, AT8, and PHF1) or (1:500) (RTM38 and GFP) diluted with blocking buffer were incubated overnight at 4 °C and washed with PBS. Subsequently, secondary antibodies (1:2000) (Goat anti-Mouse IgG (H + L) Secondary Antibody/Alexa Fluor 647, Goat anti-Rabbit IgG (H + L) Secondary Antibody/Alexa Fluor 488, Goat anti-Rabbit IgG (H + L) Secondary Antibody/Alexa Fluor 555, Goat anti-Chicken IgY (H + L) Secondary Antibody/Alexa Fluor 488, Goat anti-Rat IgG (H + L) Cross-Adsorbed Secondary Antibody/Alexa Fluor 647) and 10 μg/ml Hoechst 33,342 diluted with blocking buffer were incubated for 1 h at room temperature. After washing with PBS, fluorescence (excitation 545 nm/emission 605 nm, excitation 620 nm/emission 700 nm, or excitation 360 nm/emission 460 nm) was observed with the fluorescence microscope BIOREVO BZ-X800 (Keyence) or IN Cell Analyzer 6000 (GE Healthcare).

2.7. Western blotting

Cell lysates were obtained by dissolving neurons with mRIPA buffer containing protease and phosphatase inhibitors. After sonication, the lysates were centrifuged at 15,000×*g* for 5 min. Protein concentration was measured by Bicinchoninic Acid (BCA) assay. Cell lysates (including 3 μg protein per lane for fluorescence detection, or 4.4 μg protein per lane for ECL detection) and tau protein ladder were loaded onto Extra PAGE One Precast Gels 5–15 %. After SDS-PAGE, the proteins were transferred onto Immobilon-FL PVDF membranes. After blocking with 5 % skim milk, 5 % BSA or Odyssey Blocking Buffer for 30 min, the membrane was incubated overnight at 4 °C with primary antibodies (βIII tubulin, Actin, NR2B, GFP, total tau (DAKO Tau), 3R tau, 4R tau, AT8, and PHF1) diluted with Odyssey Blocking Buffer (1:2000). After three times of 1 × TBST wash, the membranes were incubated with secondary antibodies (1:10,000) (IRDye 680RD Donkey anti-Mouse IgG, IRDye 680RD Donkey anti-Rabbit IgG, IRDye 800CW Donkey anti-Mouse IgG, IRDye 800CW Goat anti-Mouse IgG and IRDye 800CW Donkey anti-Rabbit IgG) or (1:5000) (Peroxidase AffiniPure Donkey anti-Mouse IgG (H + L), Peroxidase AffiniPure Goat anti-Rabbit IgG (H + L)) diluted with Odyssey Blocking Buffer for 1 h. After three times of 1 × TBST wash, protein bands were detected by Odyssey CLx (LI-COR, Lincoln, NE, USA), or emitted band signal using ECL prime were detected by CCD camera-based quantitative biomolecular imager ImageQuant LAS 4000 mini (GE Healthcare).

2.8. Ca^{2+} imaging

The iPSC-derived neurons were incubated with 4.7 μM Ca^{2+} indicator Fluo-8 AM (AAT Bioquest) and 0.02 % Cremophor for 10 min, and the medium was replaced with the 1x recording medium. 100 μM NMDAR antagonist MK-801 was added into 1x Recording buffer 1 min before measurement.

Fluo-8 fluorescence intensity was captured as 301 streaming images at 0.75-s intervals using an IX83 inverted microscope (Olympus, Tokyo, Japan) equipped with a 20× objective lens, filter sets (excitation 460–480 nm, emission 495–540 nm, and dichroic mirror 490 nm), an Electron Multiplying CCD Camera (Hamamatsu Photonics, Hamamatsu, Shizuoka, Japan) and LED illumination system pE-4000 (CoolLED, Andover SP10 5NY, UK).

The Fluo-8 fluorescence traces were analyzed by MetaMorph® Microscopy Automation and Image Analysis Software (Molecular Devices, San Jose, CA, USA) or Image J (ver 1.50i). Each ROI (region of

interest) was placed on each neuron, and 34–40 ROIs were analyzed in one image field. More than 120 ROIs were analyzed in total for each condition. The total fluorescence intensity in each ROI at time t was subtracted by the background fluorescence intensity, defined by the fluorescence intensity of the ROI without cell, was defined as F_t. To eliminate the possibility of encountering Ca^{2+} transients in the first frame; we selected F_{base} from the frame with the lowest signal within the first 1 min for each ROI as previously described [23].

The rate of increase/decrease of F_t concerning F_{base} ($\Delta F/F_{base}$ (%)) was calculated as $(F_t - F_{base})/F_{base}$ (%). Spontaneous oscillations of neuronal cells were analyzed by Ca^{2+} transient. Ca^{2+} transient was defined as an event in which $\Delta F/F_{base}$ (%) increased by 10 % or more and then decreased by 10 % or more, and the frequency of Ca^{2+} transients in each ROI was measured. The value obtained by dividing the obtained Ca^{2+} transient number by the image acquisition time of 3.75 (min) was calculated as the frequency of Ca^{2+} transient (min^{-1}). Image J was used to create 30 frames/sec video files for one field of view in each group.

2.9. Proximity ligation assay (PLA)

Tau–Fyn interaction was detected by the PLA method according to the manufacturer protocol with minor modifications (Duolink PLA fluorescent protocol). Cells were fixed and performed blocking in the same method of immunofluorescence. Tau (HT7 antibody) -Fyn interaction and GFP-tau expression were examined by IN Cell Analyzer 6000 or BIOREVO BZ-X800, and the number of foci was quantified with Image J (ver 1.50i) described as below.

The foci observed in each image were extracted using Image J. In addition, the cell area containing neurites was extracted as green fluorescence emitted by GFP-tau fusion protein expressed in neurons. The tau-Fyn PLA foci/GFP-tau area was calculated as an indicator of tau-Fyn interaction.

2.10. Bulk RNAseq analysis

2–5 μg of total RNA from each sample was purified using RNAeasy kit (Qiagen). After we confirmed the quality of the purified RNA using Bioanalyzer, the mRNA libraries were prepared in a strand-specific manner using NEBNext Poly(A) mRNA Magnetic Isolation Module (Cat No. E7490) and NEBNext UltraTMII Directional RNA Library Prep Kit (Cat No. E7760) and sequenced using NovaSeq 6000 (Illumina) to obtain 150-bp paired-end reads. Raw reads were trimmed based on the read quality and read length using FastQC version 0.11.7 and Trimmomatic version 0.38, respectively. The RNA-seq data were mapped to the corresponding genomic DNA sequences (human [GPCh38]) using HISAT2 version 2.1.0. The read counts, fragments per kilobase of exon per million mapped fragments (FPKM), and transcripts per million (TPM) were calculated using featureCounts version 1.6.3. The samples were clustered with the Wald method based on Euclidean distances of the normalized counts using stats (Version 3.6.1) and gplots (Version 3.0.1.1) R packages. The differentially expressed genes were detected using DESeq2 version 1.30.1. Enrichment of GO (gene ontology) biological process and correlation network of enriched GO terms was used clusterProfiler package version 3.18.1 [24] with 0.01 and 0.05 as p-value and q-value (BH methods) cut-off values.

2.11. Statistical analysis

The statistical tests used for each dataset are specified in the figure legends. Statistical analyses were done with Prism 5.04, 7, 9 or 10. Normality was assessed with the Shapiro–Wilk normality test. Variances were evaluated with the F-test (two groups) or Bartlett's test (more than two groups). A two-tailed t-test was used for most comparisons of two groups with Gaussian distribution and equal variances. P-values were adjusted with the Holm correction for multiple comparisons for individual pairs in a dataset. The two-tailed unpaired t-test or Mann–Whitney test was used to compare two groups with normal distributions or non-normal distributions, respectively. For multiple group comparisons with non-normal distribution, we used one-way ANOVA with post hoc Tukey or Dunnett's test. For multiple group comparisons with non-normal distribution, Kruskal–Wallis test with post-hoc Dunn's test was used. Values reported are means ± SD. Differences were considered significant at $P \leq 0.05$.

3. Results

3.1. Isogenic iPSC lines with the A152T MAPT mutation were established by gene editing and differentiated into neurons by Ngn2 and miR-9/9*-124 induction

To visualize the expression of endogenous tau in living neurons, we first fused the TagGFP2 (hereafter simply GFP) coding sequence to either the 5′ or 3′ end of the *MAPT* gene (N-GFP-tau and C-GFP-tau) in a healthy control iPSC line [25], by genome-editing technology (Fig. 1A and Supplemental Figs. S1A, B, C). To differentiate the iPSCs into forebrain excitatory neurons, Ngn2 and miR-9/9*-124 were introduced, as reported previously [19] (Fig. 1B). By using the Tet-ON system using Doxycycline (DOX) to drive the expression of the introduced Ngn2 and miRNAs, the iPSCs were differentiated into neurons. GFP signals were detected in both N-GFP-tau and C-GFP-tau lines, indicating that both lines were able to differentiate into neurons, and GFP-fused tau protein was expressed in those cells (Supplemental Fig. S1D). However, the intensity of C-GFP-tau was much lower than that of N-GFP-tau, which was confirmed by Western blotting that the C-GFP-tau line expressed less GFP-tau than the N-GFP-tau line (Supplemental Fig. S1E), suggesting that the disruption of the 3' UTR of the *MAPT* gene significantly affects endogenous tau expression. Thus, in the following experiments, we utilized the N-GFP-tau line only.

Next, heterozygous and homozygous A152T or P301S *MAPT* gene mutations were introduced into the N-GFP-tau line (Fig. 1C, Supplemental Figs. S2A, B, C). In addition to those lines, tau knockout (KO) iPSC was established as a negative control by inserting the GFP-polyA sequence into the *MAPT* gene immediately upstream site of the start codon (Fig. 1D, Supplemental Fig. S2D). In total, six iPSC lines were established in this study (N-GFP-tau (WT/WT), C-GFP-tau (WT/WT), WT/A152T, A152T/A152T, P301S/P301S, and KO-tau) (Supplemental Figure Table S2).

iPSC-derived neurons of each WT/WT, A152T/A152T, P301S/P301S lines showed similar GFP-tagged tau expression levels(Fig. 1E and F). The GFP expression level in the tau KO line, where the *MAPT* gene was replaced with GFP at the downstream of the promoter of the *MAPT* gene, was lower compared to the other lines(Fig. 1E and F). This suggests that the half-life of tau-conjugated GFP is longer than that of GFP alone [26,27]. The immunocytochemistry showed that NeuN and MAP2 positive cell rates, which indicate neuronal maturation, were around 90 % across the four lines (Fig. 1G and H). The fluorescent intensity of mRFP, encoded in the plasmid construct harboring miR-9/9*-124, has a minimum effect on the observation of red fluorescence signals after immunostaining (Supplemental Fig. S3A).

In neurons derived from the WT/WT, WT/A152T, and A152T/A152T iPSC lines, tau expression and phosphorylation were detected using pan-tau and phosphorylation-dependent antibodies. The lack of staining by these antibodies in KO/KO iPSCs-derived neurons indicated the specificity of these signals (Fig. 2A). Co-labeling of

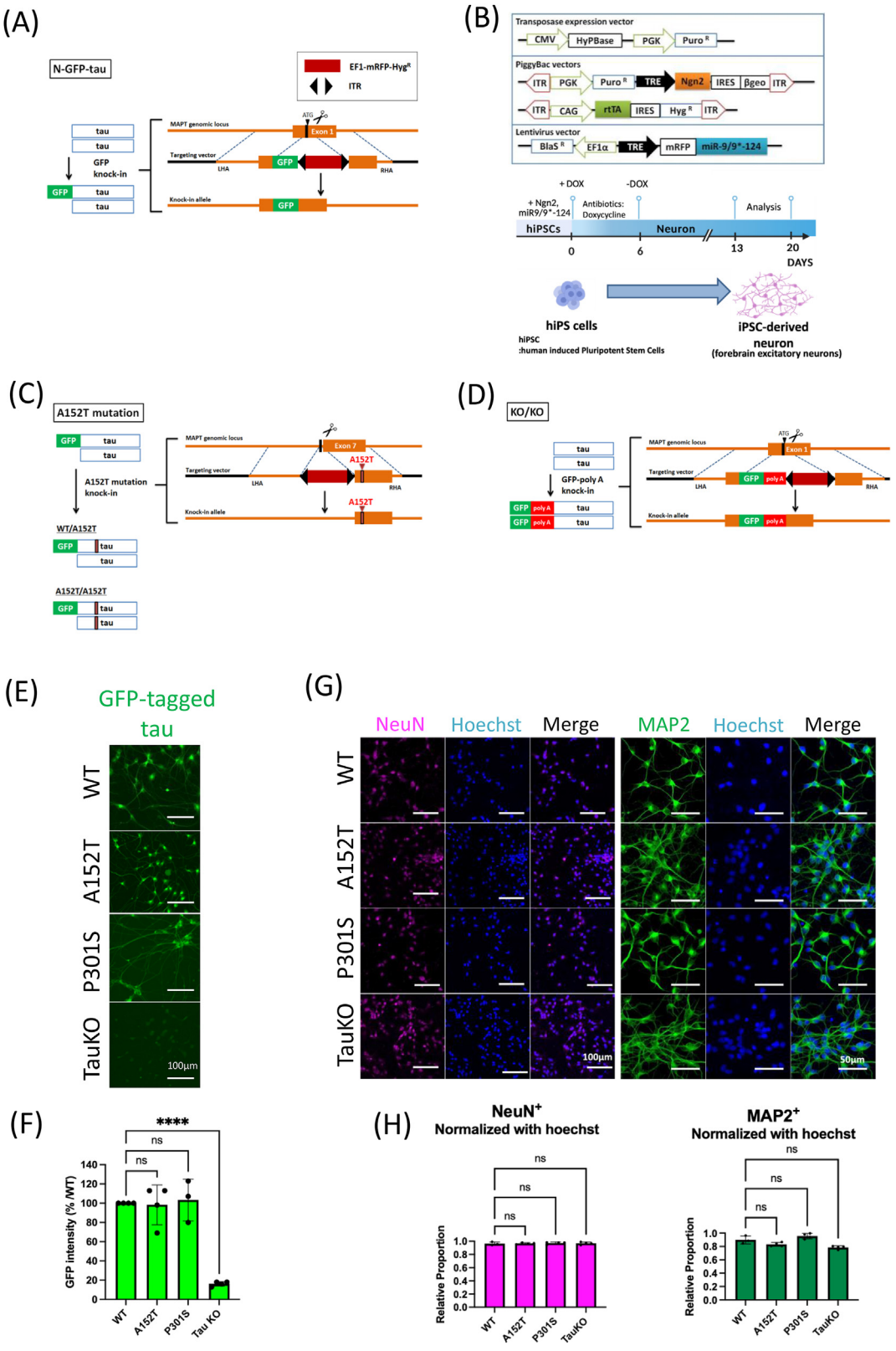

Fig. 1. Isogenic iPSC lines are established by gene editing and differentiated to neurons by Ngn2 and miR-9/9*-124 induction. (A–D) Schematic diagrams of TagGFP2 gene (GFP) insertion into the N-terminal of the *MAPT* gene (A), vectors and timeline for neuronal differentiation (B), knock-in of the A152T *MAPT* gene mutation using a targeting vector (C), insertion of GFP-poly A into the N-terminal for *MAPT* gene knockout (D). (E) GFP-tagged tau expression of each WT, A152T, P301S, and KO iPSC-derived neurons. The tau expression level was estimated by GFP-tau fluorescence without immunolabeling (day 15). Scale bar; 100 μm. (F) The relative proportion (%) of GFP-tagged tau intensity compared to the WT line (n = 3 for WT and P301S, and 4 for A152T and TauKO). Bars, mean ± SEM. ns (not significant): $P > 0.05$, ****: $P \leq 0.0001$ by Kruskal–Wallis test with Dunn's multiple comparison test. (G) Immunocytochemistry images of iPSC-derived neurons at day 15 after neuronal induction stained with mature neuron markers NeuN (magenta), MAP2 antibodies (green), and Hoechst 33,342 (blue). Scale bars; 100 μm (NeuN) and 50 μm (MAP2). (H) The relative proportion of NeuN and MAP2 positive cells compared to Hoechst (n = 3). Bars, mean ± SEM. ns (not significant): >0.05 by Kruskal–Wallis test with Dunn's multiple comparisons test.

MAP2, tau, and GFP fused to tau demonstrated that tau localized not only in axons but also in dendrites of these neurons (Fig. 2B), indicating that in these neurons, the subcellular localization of endogenous tau is not restricted to axons as recognized in immature or tauopathy neurons [28,29]. Additionally, neurites started to extend immediately after the DOX treatment, while tau expression eventually increased one week later (Fig. 2C). It suggests that tau expression is not essential for neurite extension, consistent with the previous studies of murine *Mapt* deletion [10]. The comparable level of neurite extension in tau KO neurons to that of control neurons also supports this idea (Fig. 1G).

Furthermore, the expressions of tau and neuronal markers (βIII tubulin and NR2B) in iPSC-derived neurons were confirmed by Western blotting (Fig. 2D). Antibodies against total tau, 3R tau, and phosphorylated tau (AT8, PHF1) detected dual bands corresponding to normal tau and GFP-fused tau, respectively, in WT/WT, WT/A152T, and A152T/A152T neurons, indicating that GFP-tagged wild-type and mutated tau proteins were expressed as 3R tau and phosphorylated. Quantitative data revealed the comparative levels of total tau expression and the relative proportion of phosphorylated tau (PHF1) to total tau in WT/WT, WT/A152T, and A152T/A152T neurons, while no tau expression was detected in KO neurons (Supplemental Fig. S3B), indicating that these expressions were not affected by *MAPT* deletion or A152T mutation. Considering that the bands recognized by 4R tau were non-specific bands that were also detected in KO cells (Fig. 2D and Supplemental Fig. S3C), 4R tau expression is low in these cells. In the neurons carrying the P301S/P301S mutation (Supplemental Fig. S2C), tau antibodies detected doublet bands corresponding to 3R and 4R tau with or without the GFP-tag based on the molecular weight (Supplemental Fig. S3C), indicating that only P301S mutation drove the expression of 4R tau.

3.2. hTau-A152T expression increases neuronal excitation in iPSC-derived neurons

Previously, the exon10 + 16 and R406W *MAPT* gene mutations are reported to increase the response to electrical stimulation [18]. In addition, the hTau-A152T expression in mouse brains increased spontaneous neuronal excitation [9]. To examine excitability in unstimulated human neurons expressing hTau-A152T, we visualized Ca^{2+} oscillation by a fluorescence indicator, Fluo-8. The frequency of Ca^{2+} oscillation was increased in A152T/A152T neurons compared to WT/WT neurons (Fig. 3A, Supplemental Fig. S4 and Supplemental Movie). All the neurons used in these experiments express GFP fused to the *MAPT* gene, but the GFP fluorescence was at a negligible level compared to the Fluo-8 fluorescence (Supplemental Fig. S5A). To exclude the possibility that the non-targeting effect of genome editing affected neuronal excitability, we knocked down tau expression by exposing neurons to anti-Tau siRNA and examined the Ca^{2+} oscillation (Fig. 3B). GFP signal indicated that anti-Tau siRNA treatment started to suppress tau expression soon after it was added on day 6, and then reached down to around 20 % signal plateau within 2 weeks (Supplemental Fig. S5B). The anti-Tau siRNA reduced Ca^{2+} oscillation frequency in both WT/WT and A152T/A152T neurons (Fig. 3C), suggesting that both tau expression and the A152T mutation contribute to the Ca^{2+} oscillation in the hiPSC-derived neurons.

Tau reduction was reported to have differential effects not only on excitatory neurons but also on inhibitory neurons [30]. Thus, we aimed to examine *MAPT* gene mutation effects on inhibitory neurons. We differentiated the iPSCs into the neuronal culture mainly composed of inhibitory neurons (Fig. 3D). In the inhibitory neuron-enriched culture, we found that Ca^{2+} oscillation frequency decreased compared to the WT control (Fig. 3D). These observations suggest that the A152T mutation increases the activity of excitatory neurons in the inhibitory neuron-enriched culture, which in turn activates inhibitory neurons abundant in this culture and ultimately reduces the oscillation of Ca^{2+} in the entire system.

3.3. The tau-Fyn-NMDA receptor pathway is involved in the increased neuronal excitability by hTau-A152T

Tau modulates NMDA receptor (NMDAR)-dependent excitotoxicity in mouse primary neuronal culture [31,32]. To examine the involvement of NMDAR in the increased neuronal excitation in A152T/A152T neurons, we treated A152T/A152T neurons with NMDAR antagonist MK-801 to block NMDAR-dependent signals. As a result, Ca^{2+} oscillation was almost completely suppressed by MK-801 treatment, and similarly, in WT/WT neurons, MK-801 treatment suppressed Ca^{2+} oscillation (Fig. 4A). These results indicate that neuronal excitation is mediated by NMDA receptors in both WT/WT and A152T/A152T neurons.

Next, we analyzed the intracellular interaction of tau and tyrosine kinase Fyn, a key regulator of NMDAR, by proximity ligation assay (PLA). We found that PLA using tau and Fyn antibodies labeled only a subset of tau (Fig. 4B). The number of PLA foci visualized by tau and Fyn antibodies was increased in A152T/A152T neurons compared to WT/WT neurons (Fig. 4B). Signals shaping the nuclei in PLA (Fig. 4B blue arrow) were observed in all three cell lines including tau KO neurons, indicating that these signals in nuclei are not due to tau-Fyn interaction but artifacts of the assay. Concomitant visualization of GFP and PLA signals indicated that only a subset of tau interacts with Fyn. The number of punctate staining per area of these neurons was increased in A152T neurons compared to WT neurons (Fig. 4C). These findings indicate that tau-Fyn interaction is increased in A152T/A152T neurons compared to that in WT/WT neurons. This suggests that the hyperexcitability of the A152T mutant neurons is mediated by the tau-Fyn-NMDAR pathway.

3.4. hTau-A152T mutation causes structural change in hiPSC-derived excitatory neurons

We also searched for the molecular mechanisms of hTau-A152T-induced activation of excitatory neurons using transcriptome analysis. In PCA and heatmap, hTau-A152T/A152T neurons were closest to hTau-WT/WT neurons, while hTau-P301S/P301S and hTau-KO/KO neurons were separated from them (Fig. 5A and B). In the volcano plot of hTau-WT/WT over hTau-A152T/A152T neurons, neuronal activity-dependent genes like Myc were upregulated, while structural changes were indicated by the upregulation of HOXB9 and IRX2 (Fig. 5C). Consistent with those changes in the volcano plot, gene ontology (GO) analysis of differentially expressed genes (DEGs) revealed top GO terms indicating structural changes like axon development, though we could not observe significant differences among hTau-WT/WT and hTau-A152T/A152T neurons (Fig. 5D). In addition, the top 10 GO terms of common DEGs between WT and A152T or P301S lines are shown in Supplemental Fig. 6. The nuclear/mitotic division-related genes such as *Ascl1* and *Klf4* were included, indicating that tau mutations accelerate cell proliferation and cell cycle progression, leading to pathological changes.

4. Discussion

Clinically, tau-related neurodegenerative disorders such as AD, FTD, and DLB increase the risk of developing new-onset epilepsy [2,33,34]. While most *MAPT* mutations are exclusively linked to

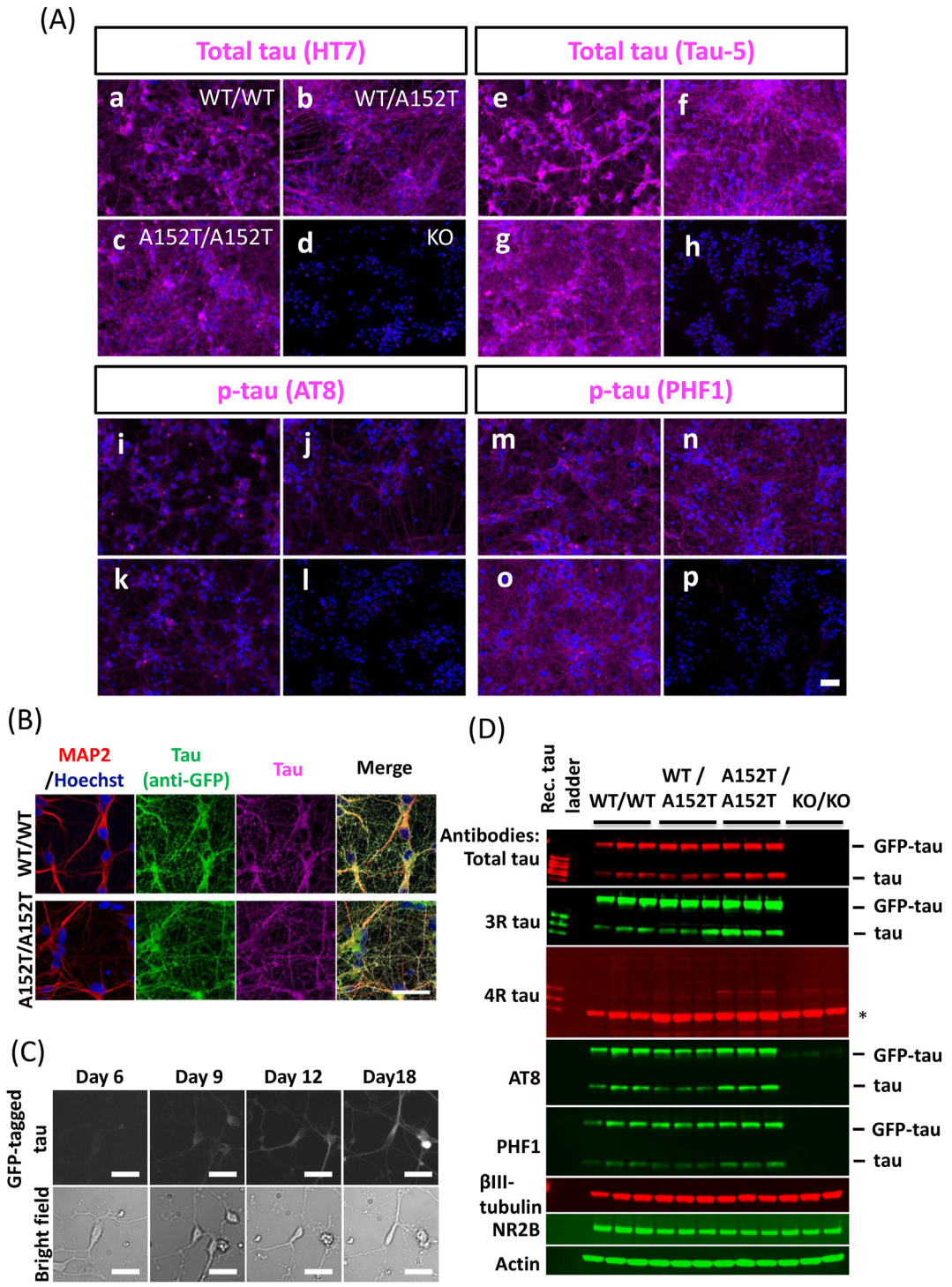

Fig. 2. Endogenous tau distribution and phosphorylation. (A) Immunofluorescence analysis of neurons at day 23 after neuronal induction using total tau (HT7 and Tau-5), phospho-tau (AT8 and PHF1) antibodies. a, e, i, m: WT/WT; b, f, j, n: WT/A152T; c, g, k, o: A152T/A152T; d, h, l, p: KO. Scale bar; 50 μm. (B) Co-labeling of neurons with MAP2 (red), Hoechst 33,342 (blue), GFP (green), and Tau (magenta) in WT/WT (upper) or A152T/A152T (lower) neurons at day 23 indicated overlapping signals of tau and MAP2 staining in dendrites. Scale bar; 40 μm. (C) Tau expression in identical neurons was visualized by GFP conjugated with tau protein (upper panels) at the indicated days after induction. Neurite extension was visualized by a bright field (lower panels) and compared with the GFP intensity. Scale bars; 30 μm. (D) Western blotting analysis of day 20 neurons using total-tau (Tau-5), 3R tau, 4R tau, phospho-tau (AT8 and PHF1), βIII tubulin, NR2B, and Actin antibodies (n = 3). Asterisk (*) indicates a non-specific band signal.

frontotemporal lobar degeneration (FTLD), the rare *MAPT* gene variant A152T is an exception, identified as a genetic risk factor for both FTLD and AD [13,35]. Thus, studies on the A152T mutation will offer valuable insights into tau pathogenesis in AD. Studies utilizing animal models have provided insights into the involvement of the A152T mutation in hyper-excitation of neurons. In transgenic mice overexpressing human *MAPT* with the A152T mutation, the elevated extracellular glutamate levels triggered NMDAR-mediated neurotoxicity [36,37]. This excitotoxicity results in intracellular calcium dyshomeostasis [38], and enhanced neuronal

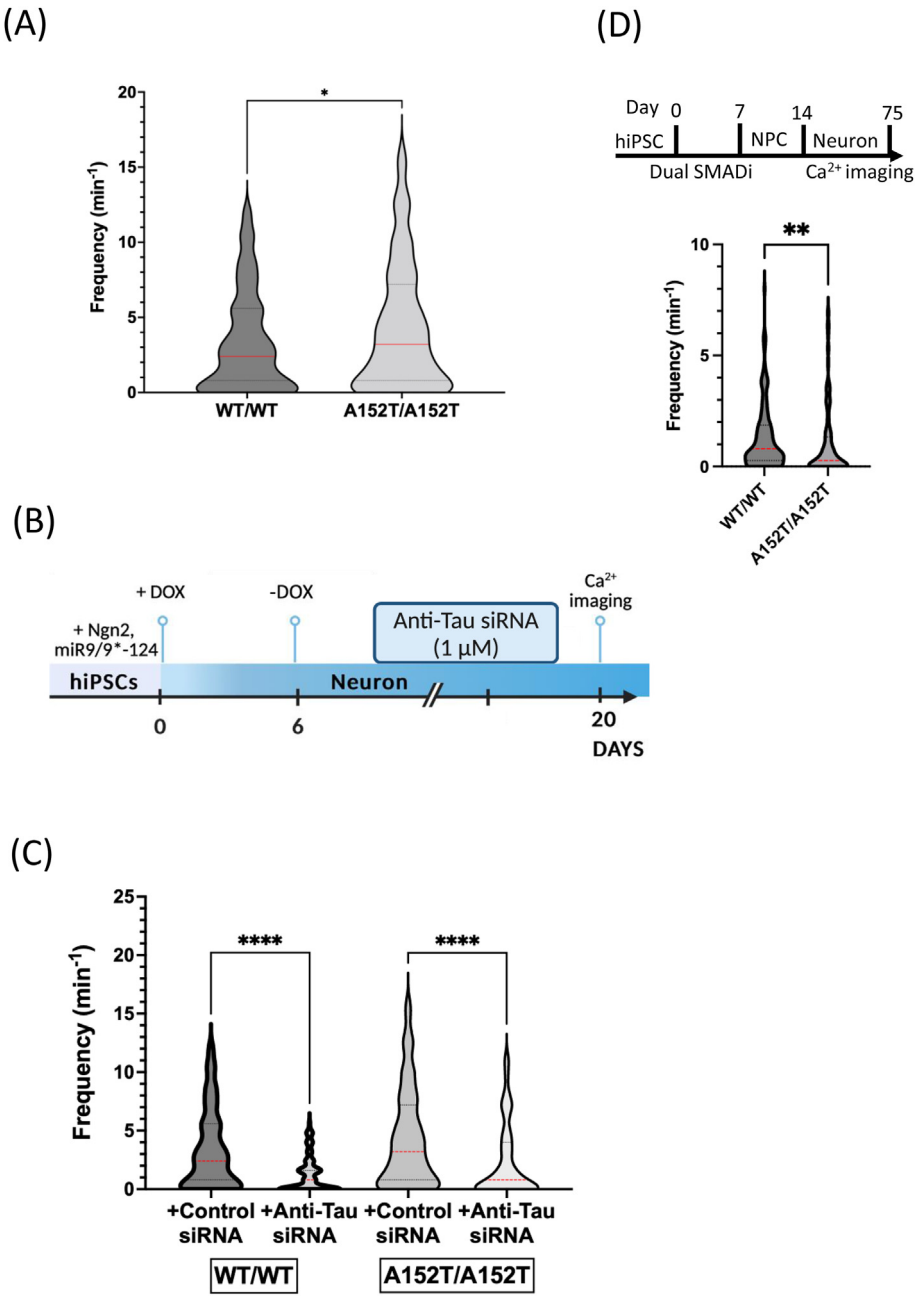

Fig. 3. hTau-A152T increases neuronal excitation. (A) Increased Ca^{2+} transients due to hTau-A152T mutation in unstimulated neurons at day 20 after neuronal induction. Red bars: median of n = 208(WT) or 292(A152T) ROIs. *: P ≤ 0.05 by Kruskal–Wallis test with Dunn's multiple comparisons test. (B, C) WT/WT and A152T/A152T neurons were treated with 1 μM anti-Tau siRNA (Anti-Tau siRNA) or non-targeting siRNA control (Control siRNA) for two weeks (B). Neuronal excitation was measured by frequency of Ca^{2+} oscillation in Fluo-8 imaging analysis 20 days after neuronal induction. The oscillation frequency of WT and increased frequency by hTau-A152T compared to WT were suppressed by anti-Tau siRNA (C). Red bar: median of n = 208 (WT/WT + Control siRNA), 160 (WT/WT + Anti-Tau siRNA), 292 (A152T/A152T + Control siRNA), or 138 (A152T/A152T + Anti-Tau siRNA), or ROIs, respectively. ****: P ≤ 0.0001 by Kruskal–Wallis test with Dunn's multiple comparisons test. (D) Inhibitory neuron-enriched cultures from WT/WT and A152T/A152T hiPSCs were generated using dual SMAD inhibition through neuronal precursor cells (top). After two months of neuronal culture, Ca^{2+} oscillations were assessed in the mixed culture (bottom). Red bars: median of n = 160(WT/WT) or 150(A152T/A152T) ROIs. **: P ≤ 0.01 by Mann–Whitney test.

responsiveness to synaptic electrical stimulation and epileptogenic chemicals, leading to spontaneous nonconvulsive epileptiform activity [9]. Consequently, alterations are associated with progressive neuronal loss, particularly affecting the glutamatergic system [9,38]. Furthermore, transgenic *Caenorhabditis elegans* expressing the A152T variant exhibit severe paralysis accompanied by acute neuronal dysfunction and pan-neuronal locomotor deficits [38,39].

Although those studies using animal models provide compelling insights into the A152T mutation-dependent pathogenesis, the complexities of cellular signaling processes and genetic variability between the model and human or within human individuals should be validated using human cellular models. For example, *C. elegans* neurons have ion channels but not voltage-gated sodium channels [40], necessitating further investigation in human cell-derived systems [41]. Studies using iPSC models harboring the A152T mutation have described increased sensitivity to stress-induced cell death [14,15], though no report revealed neurodegeneration via hyperexcitability by the A152T *MAPT* mutation in a human cell model.

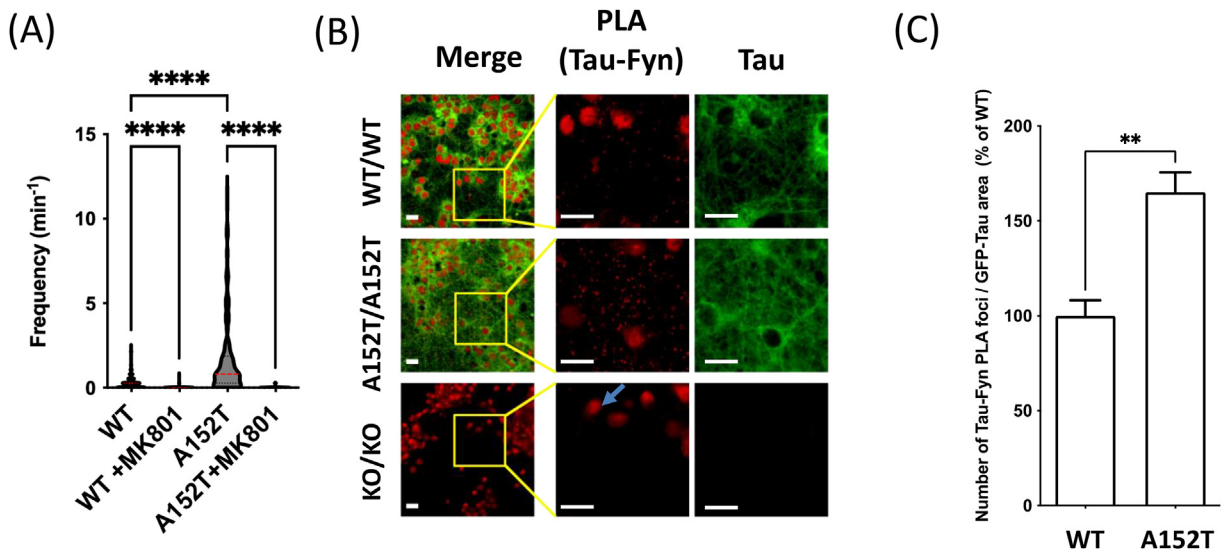

Fig. 4. The tau-Fyn-NMDA receptor pathway is involved in neuronal excitability. (A) Changes of Ca^{2+} transients due to the effect of NMDAR antagonist MK-801 in WT and A152T neurons. WT and A152T neurons were treated with NMDA receptor antagonist MK-801 (100 μM) 1 min before measurement. Neuronal excitation was measured by frequency of Ca^{2+} oscillation in Fluo-8 imaging analysis on day 22 after neuronal induction. Red bars: median of n = 200 (WT/WT no treat, WT/WT + MK-801, and A152T/A152T no treat), or 120 (A152T/A152T + MK801) ROIs, respectively. ****: $P \leq 0.0001$ by Mann Whitney test. (B) Tau–Fyn interaction was visualized by the PLA method using total tau (HT7) and Fyn antibodies (PLA tau-Fyn) in day 20 neurons. Total tau was visualized by the GFP fluorescence (tau). PLA foci (red) represent the interaction between tau and Fyn. Only a subset of tau interacts with Fyn. Nuclear signals (a blue arrow indicates an example) are observed even in KO neurons, suggesting that these signals are non-specific. Scale bars; 20 μm. (C) Quantification of PLA foci showing intracellular interaction between tau and Fyn. The number of PLA foci was normalized by the amount of total tau visualized by GFP signals. Bars and error bars are mean +SD. n = 5 (each WT and A152T) images. *: $P \leq 0.05$ by unpaired t-test.

In this study, we introduced the *MAPT* mutations, A152T or P301S, to the hiPSC line from a healthy individual. We found that the A152T mutation induced hyperexcitability in excitatory neurons in human cells. This was reminiscent of the findings in hTau-A152T transgenic mice because hTau-A152T expression was driven in purely excitatory neurons by the *CaMKII* promoter in the hTau-A152T mice [9].

Tau–Fyn binding anchors Fyn near post-synaptic density and consequently activates NMDAR subunit NR2B [42]. In the present study, inhibition of NMDAR suppressed neuronal excitability not only in A152T/A152T neurons but also in WT/WT neurons, and tau-Fyn interaction was also observed in WT/WT neurons. Therefore, it is suggested that neuronal excitability due to the A152T mutation is caused by excessive enhancement of the physiological action of WT tau. Some *MAPT* gene mutations are reported to increase the tau-Fyn interaction affinity and stabilize Fyn to an active state (open conformation) that promotes binding within dendrites [43,44]. Though these mutation effects have not been confirmed with A152T mutation, the relative increase in tau-Fyn interaction we observed in A152T neurons possibly reflects them. Further studies are needed on how the A152T mutation activates the tau-Fyn-NMDAR pathway and induces neuronal excitability, such as phosphorylation status and intracellular localization of the tau-Fyn complex like analyzed on other *MAPT* mutations [45].

Transcriptome analysis revealed structural changes by the A152T mutation in addition to genes upregulated in an activity-dependent manner, although the A152T mutation induced fewer changes to hiPSC-neurons than KO or the P301S mutation. The increased tau-Fyn interaction observed in A152T, which may contribute to neuronal hyperexcitability, may result from changes in cell structure or from the proximity of the mutation to the tau-Fyn binding site. However, because the changes in the transcriptional profile directly responsible for the increased excitability were limited, it is more likely that the increased tau-Fyn binding caused by the A152T mutation contributes to the increased neuronal activity.

The top 10 GO terms for common DEGs between WT and A152T or P301S lines were related to nuclear/mitotic division, suggesting that tau mutations accelerate cell cycle progression, leading to pathological changes. This is consistent with the evidence from both familial AD iPSC-derived neurons and post-mortem AD brain tissue, indicating that early in disease progression, neurons show signs of dedifferentiation towards progenitor-like states, induce hypo-mature neuronal identity characterized by stress markers, re-enter the cell cycle, and become dysfunctional, lacking the resilience of mature neurons [46–49]. Taken together, these findings suggest an aberrant neuronal transformation and age- or mutation-related epigenetic deterioration. In addition, the P301L mutation of the *MAPT* gene has been reported to induce nuclear membrane deformation and defective nucleocytoplasmic transport [49]. Thus, we also successfully recapitulate the previously reported tau-dependent pathogenesis. However, further studies are needed to clarify how these common changes between A152T and P301S influence the A152T-specific changes.

Our study reproduced tau-dependent neuronal excitability in iPSC-derived neurons by the A152T mutation, suggesting the tau-Fyn-NMDAR pathway as a molecular mechanism of neuronal excitability. Additionally, Tau reduction by anti-Tau siRNA suppressed the increased excitability by A152T, thus tau reduction is expected to be a treatment for neurodegeneration in tau-related diseases and epileptic symptoms. Further research on the mechanisms of tau-dependent hyperexcitability will help to establish therapeutics for the progression of neurodegenerative disease as well as epilepsy in dementia. Though the effect of complete *MAPT* gene knockout is still controversial, some reports point out important issues, such as developing age-dependent motor and cognitive deficits in a mouse model [50]. It is also reported that in *MAPT*-depleted human iPSCs-derived cortical neurons, both neuronal activity and neurite outgrowth were impaired [51]. Our study similarly demonstrated that anti-Tau siRNA decreased the Ca^{2+} oscillation frequency not only in A152T neurons but also in WT neurons. These findings suggest that while tau reduction counteracted

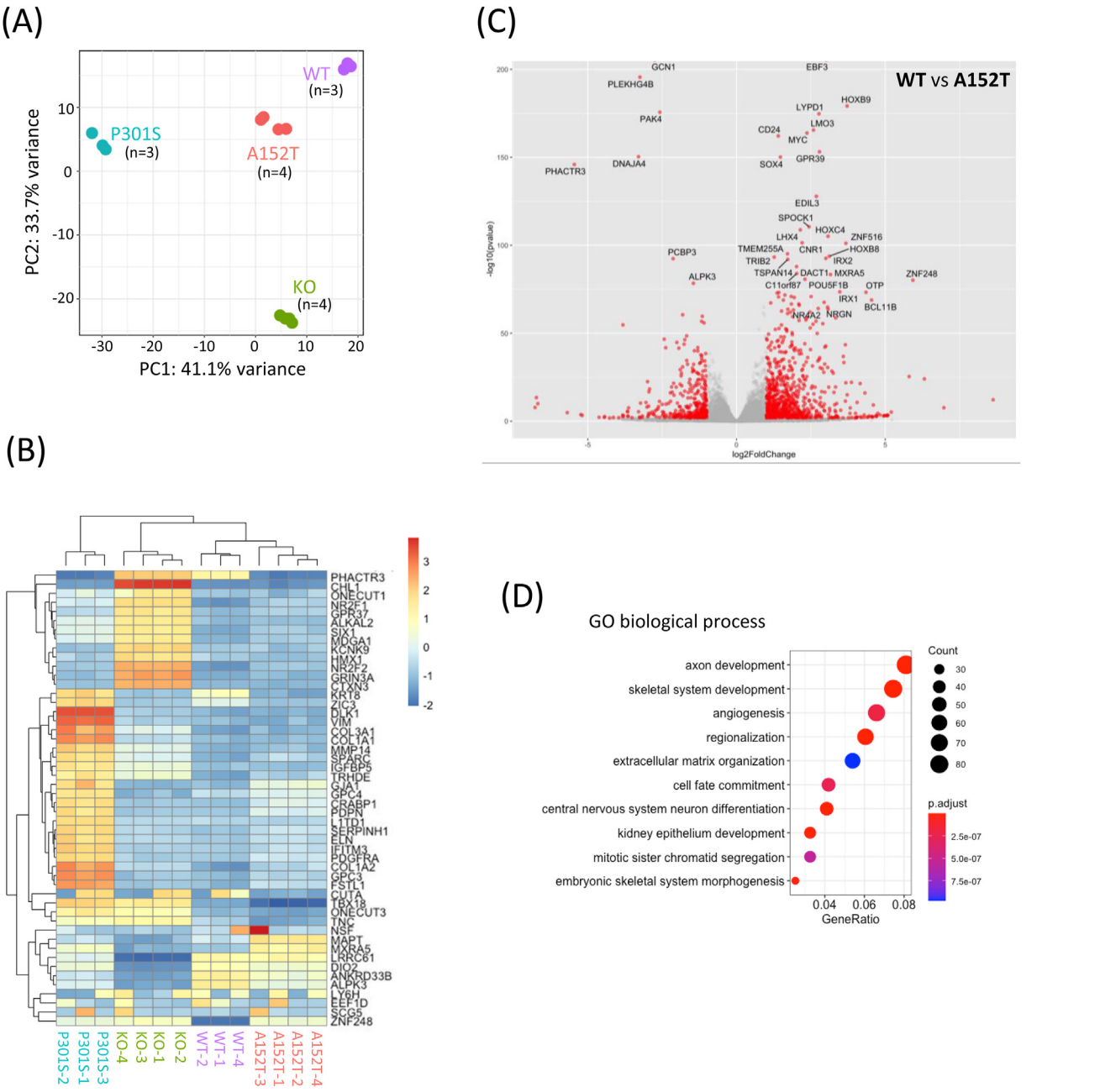

Fig. 5. Transcriptome analysis of hiPSC-derived excitatory neurons. (A) RNA samples of hiPSC-derived excitatory neurons were recovered at day 14 after neuronal induction and analyzed by RNAseq. The hTau-WT/WT, A152T/A152T, P301S/P301S, and KO/KO neurons are indicated as WT, A152T, P301S, and KO, respectively. The PCA analysis of RNAseq (N = 3 for WT, 4 for A152T, 3 for P301S, and 4 for KO) indicated that A152T induces fewer changes compared to KO or P301S. (B) The heat map of individual samples also indicated that the expression pattern of hTau-A152T neurons is the closest to that of hTau-WT neurons. The box colors indicate the magnitudes of gene-expression fold changes. (C) The volcano plot of A152T versus WT indicated differentially expressed genes (DEGs) including immediate early genes like MYC. The right side indicates the upregulated genes in hTau-A152T neurons, while the left side indicates the upregulated genes in hTau-WT neurons. The top 50 genes that showed the lowest p-values are labeled. (D) Gene Ontology (GO) analysis of the DEGs in the comparison of hTau-WT and hTau-A152T neurons indicated that structural changes like axon development or central nervous system neuron differentiation are induced by A152T mutation.

hyperexcitability caused by the A152T mutation, either knockout or knockdown of tau can result in functional deficits.

Therefore, in future drug screenings aiming at modulating tau expression levels, it will be crucial to target pathogenic tau species or achieve moderate tau reduction to preserve normal neuronal function. For this purpose, the iPSC models we developed offer a substantial advantage, as they incorporate *MAPT* mutations alongside a fluorescent protein fused to tau, enabling real-time monitoring of endogenous tau expression levels and its subcellular localization before and after drug treatment.

5. Limitations of this study

Epilepsy often arises from complex interactions between various neural cell types, including neurons and glia. Neuron monocultures derived from iPSCs typically fail to exhibit synchronous network activity unless co-cultured with human or murine astrocytes [52], limiting their utility in modeling network disturbances associated with epilepsy. However, recent advancements in 3D culture techniques have enabled the generation of cerebral organoids containing various types of neural cells, where

spontaneous and synchronized neural activity can be observed [53–55]. These organoids hold significant promise for modeling both network-level and cell-autonomous defects in epilepsy [56]. To further investigate the neuronal hyperactivity associated with *MAPT* gene mutations, the use of electrophysiological techniques beyond Ca^{2+} imaging, such as whole-cell patch-clamp recordings or multielectrode array assays, will enhance the scope and effectiveness of our research.

While we successfully recapitulated the previously reported tau-dependent pathogenesis, the transcriptional profile changes directly responsible for the increased excitability were limited. Further studies are necessary to clarify how the shared alterations between A152T and P301S mutations or A152T-specific transcriptional changes contribute to these phenotypes especially the hyperexcitability of neurons.

The A152T mutation increased the tau-Fyn interaction. However, to determine whether this increased interaction directly contributes to the increased neuronal excitability, further studies are needed to inhibit the interaction between hTau-A152T and Fyn.

Additionally, we were unable to replicate the neuronal cell loss observed in human A152T patients. Since it takes several decades for significant neuron reduction to occur in patients, aging-related factors or stress-inducers are likely necessary to accurately mimic these neurodegenerative phenotypes.

6. Conclusion

We differentiated hiPSCs in which *MAPT* mutation A152T or P301S were introduced, into excitatory neuronal culture or inhibitory neuron-enriched culture. Using this culture systems, we showed that the A152T *MAPT* mutation increases neuronal activity in excitatory neurons. Furthermore, it was suggested that the tau-Fyn-NMDAR pathway contributes to the increased neuronal excitability of the A152T *MAPT* mutant neurons. Comprehensive transcriptomics revealed that structural changes to elevate neuronal activity were induced by the A152T mutation.

Author contributions

Maika Itsuno: Data curation; data analysis; funding acquisition; investigation; visualization; manuscript writing; project administration. **Sumihiro Maeda**: Conceptualization; data curation; data analysis; supervision; funding acquisition; investigation; visualization; methodology; manuscript writing; project administration. **Hirokazu Tanabe**: Data curation; data analysis; investigation; visualization; methodology; manuscript writing; project administration. **Etsuko Sano**: data curation; visualization. **Takashi Sasaki**: Data analysis; visualization. **Chisato Oyama**: Data curation; visualization. **Hiroko Bannai**: data curation; supervision. **Koichi Saito**: Investigation; visualization; methodology. **Kazuhiko Nakata**: Investigation; visualization; methodology. **Setsu Endoh-Yamagami**: Conceptualization; data analysis; manuscript writing; supervision. **Hideyuki Okano**: Conceptualization; funding acquisition; supervision.

All authors have read and approved the manuscript.

Data availability statement

The bulk RNA-seq datasets have been deposited in the NCBI's Gene Expression Omnibus and are accessible through GEO Series accession number GSE225864. Any additional information required to reanalyze the data reported in this article is available from the lead contact on request.

Ethics statement

The study was conducted per the Declaration of Helsinki, approved by the Ethics Committee for Human Research of the Keio University School of Medicine (#20080016).

Declaration of competing interest

The authors declare the following financial interests/personal relationships which may be considered as potential competing interests:This research project was conducted in collaboration with Keio University and Fujifilm Corporation. H.T., K.S., K.N., and S. E.-Y. are employees of Fujifilm Corporation. H.O. is a founder scientist and a Scientific Advisory Board Member for SanBio Co., Ltd., and K Pharma Inc. H.T., S. E.-Y., S. M., and H.O. are inventors on a patent application (JP 2021-61793, US2022-0326225) for "PLURIPOTENT STEM CELL, NERVE CELL, AND APPLICATION THEREOF". The remaining authors declare no conflicts of interest.

Acknowledgements

We thank Minoru S.H. Ko, Nakatake Yuki (Keio University), and Andrew S. Yoo (Washington University School of Medicine) for providing the materials. We would also like to thank Hirofumi Suemori, Shinya Yamanaka, Keisuke Okita, and Makoto Nakagawa (Kyoto University) for kindly providing 201B7 hiPSCs. We also thank all the laboratory members of H.O., especially Mitsuru Ishikawa, Hirotaka Watanabe, and Hiroyuki Miyoshi, and all the iPSC group members of Fujifilm, especially Akira Nabetani, Hitoshi Suzuki-Masuyama, and Euikyung Shin for their helpful comments, encouragement, and generous support during this study.

Some of the figures were created with BioRender.com.

This work was supported by grants from The Keio University Doctorate Student Grant-in-Aid Program from Ushioda Memorial Fund to M.I., JST SPRING, Grant Number JPMJSP2123 to M.I., Keio Global Research Initiative, Keio Gijuku Academic Development Funds, and Keio Gijuku Fukuzawa Memorial Fund for the Advancement of Education and Research to S.M., JSPS KAKENHI Grant Number JP21K06376 to S.M., JP21H02450 to S.M and H. B., JP20H00485 and JP21H05273 to H.O., the Research Center Network for Realization Research Centers/Projects of Regenerative Medicine (the Program for Intractable Disease Research Utilizing Disease-specific iPS Cells and the Acceleration Program for Intractable Diseases Research Utilizing Disease-specific iPS Cells) from the Japan Agency for Medical Research and Development (AMED) (grant no. JP22bm0804003 to H.O.), and from Fujifilm corporation.

Appendix A. Supplementary data

Supplementary data to this article can be found online at https://doi.org/10.1016/j.reth.2024.12.009.

References

[1] Vossel KA, Tartaglia MC, Nygaard HB, Zeman AZ, Miller BL. Epileptic activity in Alzheimer's disease: causes and clinical relevance. Lancet Neurol 2017;16(4):311–22. https://doi.org/10.1016/S1474-4422(17)30044-3.

[2] Beagle AJ, Darwish SM, Ranasinghe KG, La AL, Karageorgiou E, Vossel KA. Relative incidence of seizures and myoclonus in alzheimer's disease, dementia with Lewy bodies, and frontotemporal dementia. J Alzheimers Dis 2017;60:211–23. https://doi.org/10.3233/JAD-170031.

[3] Vossel KA, Ranasinghe KG, Beagle AJ, Mizuiri D, Honma SM, Dowling AF, et al. Incidence and impact of subclinical epileptiform activity in Alzheimer's disease. Ann Neurol 2016;80:858–70. https://doi.org/10.1002/ana.24794.

[4] Palop JJ, Mucke L. Network abnormalities and interneuron dysfunction in Alzheimer disease. Nat Rev Neurosci 2016;17:777–92. https://doi.org/10.1038/nrn.2016.141.

[5] Johnson ECB, Ho K, Yu GQ, Das M, Sanchez PE, Djukic B, et al. Behavioral and neural network abnormalities in human APP transgenic mice resemble those of App knock-in mice and are modulated by familial Alzheimer's disease mutations but not by inhibition of BACE1. Mol Neurodegener 2020;15(1):53. https://doi.org/10.1186/s13024-020-00393-5.
[6] Vossel K, Ranasinghe KG, Beagle AJ, La A, Ah Pook K, Castro M, et al. Effect of levetiracetam on cognition in patients with alzheimer disease with and without epileptiform activity: a randomized clinical trial. JAMA Neurol 2021;78:1345–54. https://doi.org/10.1001/jamaneurol.2021.3310.
[7] Roberson ED, Scearce-Levie K, Palop JJ, Yan F, Cheng IH, Wu T, et al. Reducing endogenous tau ameliorates amyloid beta-induced deficits in an Alzheimer's disease mouse model. Science 2007;316:750–4. https://doi.org/10.1126/science.1141736.
[8] Ittner LM, Ke YD, Delerue F, Bi M, Gladbach A, van Eersel J, et al. Dendritic function of tau mediates amyloid-β toxicity in alzheimer's disease mouse models. Cell 2010;142:387–97. https://doi.org/10.1016/j.cell.2010.06.036.
[9] Maeda S, Djukic B, Taneja P, Yu G, Lo I, Davis A, et al. Expression of A152T human tau causes age-dependent neuronal dysfunction and loss in transgenic mice. EMBO Rep 2016;17:530–51. https://doi.org/10.15252/embr.201541438.
[10] Morris M, Maeda S, Vossel K, Mucke L. The many faces of tau. Neuron 2011;70:410–26. https://doi.org/10.1016/j.neuron.2011.04.009.
[11] Lee SE, Tartaglia MC, Yener G, Genç S, Seeley WW, Sanchez-Juan P, et al. Neurodegenerative disease phenotypes in carriers of MAPT P.A152T, a risk factor for frontotemporal dementia spectrum disorders and alzheimer disease. Alzheimer Dis Assoc Disord 2013;27:302–9. https://doi.org/10.1097/WAD.0b013e31828cc357.
[12] Kara E, Ling H, Pittman AM, Shaw K, de Silva R, Simone R, et al. The MAPT p.A152T variant is a risk factor associated with tauopathies with atypical clinical and neuropathological features. Neurobiol Aging 2012;33:2231.e7. https://doi.org/10.1016/j.neurobiolaging.2012.04.006. 2231.e14.
[13] Coppola G, Chinnathambi S, Lee JJY, Dombroski BA, Baker MC, Soto-Ortolaza AI, et al. Evidence for a role of the rare p.A152T variant in MAPT in increasing the risk for FTD-spectrum and Alzheimer's diseases. Hum Mol Genet 2012;21:3500–12. https://doi.org/10.1093/HMG/DDS161.
[14] Biswas MHU, Almeida S, Lopez-Gonzalez R, Mao W, Zhang Z, Karydas A, et al. MMP-9 and MMP-2 contribute to neuronal cell death in iPSC models of frontotemporal dementia with MAPT mutations. Stem Cell Rep 2016;7:316–24. https://doi.org/10.1016/J.STEMCR.2016.08.006.
[15] Fong H, Wang C, Knoferle J, Walker D, Balestra ME, Tong LM, et al. Genetic correction of tauopathy phenotypes in neurons derived from human induced pluripotent stem cells. Stem Cell Rep 2013;1:226–34. https://doi.org/10.1016/J.STEMCR.2013.08.001.
[16] Nakamura M, Shiozawa S, Tsuboi D, Amano M, Watanabe H, Maeda S, et al. Pathological progression induced by the frontotemporal dementia-associated R406W tau mutation in patient-derived iPSCs. Stem Cell Rep 2019;13:684–99. https://doi.org/10.1016/J.STEMCR.2019.08.011.
[17] Silva MC, Cheng C, Mair W, Almeida S, Fong H, Biswas MHU, et al. Human iPSC-derived neuronal model of tau-A152T frontotemporal dementia reveals tau-mediated mechanisms of neuronal vulnerability. Stem Cell Rep 2016;7:325–40. https://doi.org/10.1016/J.STEMCR.2016.08.001.
[18] Imamura K, Sahara N, Kanaan NM, Tsukita K, Kondo T, Kutoku Y, et al. Calcium dysregulation contributes to neurodegeneration in FTLD patient iPSC-derived neurons. Sci Rep 2016;6:1–10. https://doi.org/10.1038/srep34904.
[19] Ishikawa M, Aoyama T, Shibata S, Sone T, Miyoshi H, Watanabe H, et al. miRNA-based rapid differentiation of purified neurons from hPSCs advances towards quick screening for neuronal disease phenotypes in vitro. Cells 2020;9:532. https://doi.org/10.3390/CELLS9030532.
[20] Takahashi K, Tanabe K, Ohnuki M, Narita M, Ichisaka T, Tomoda K, et al. Induction of pluripotent stem cells from adult human fibroblasts by defined factors. Cell 2007;131:861–72. https://doi.org/10.1016/j.cell.2007.11.019.
[21] Labun K, Montague TG, Krause M, Torres Cleuren YN, Tjeldnes H, Valen E. CHOPCHOP v3: expanding the CRISPR web toolbox beyond genome editing. Nucleic Acids Res 2019;47:W171–4. https://doi.org/10.1093/nar/gkz365.
[22] Supakul S, Hatakeyama Y, Leventoux N, Itsuno M, Numata N, Hiramine H, et al. Urine-derived cells from the aged donor for the 2D/3D modeling of neural cells via iPSCs. Aging Brain 2023;4:100101. https://doi.org/10.1016/j.nbas.2023.100101.
[23] Rui Y, Pollitt SL, Myers KR, Feng Y, Zheng JQ. Spontaneous local calcium transients regulate oligodendrocyte development in culture through store-operated ca2+ entry and release. ENeuro 2020;7:1–16. https://doi.org/10.1523/ENEURO.0347-19.2020.
[24] Wu T, Hu E, Xu S, Chen M, Guo P, Dai Z, et al. clusterProfiler 4.0: a universal enrichment tool for interpreting omics data. Innovation 2021;2(3):100141. https://doi.org/10.1016/j.xinn.2021.100141.
[25] Takahashi K, Yamanaka S. Induction of pluripotent stem cells from mouse embryonic and adult fibroblast cultures by defined factors. Cell 2006;126(4):663–76. https://doi.org/10.1016/j.cell.2006.07.024.
[26] Corish P, Tyler-Smith C. Attenuation of green fluorescent protein half-life in mammalian cells. Protein Eng 1999;12(12):1035–40. https://doi.org/10.1093/protein/12.12.1035.
[27] Sato C, Barthélemy NR, Mawuenyega KG, Patterson BW, Gordon BA, Jockel-Balsarotti J, et al. Tau kinetics in neurons and the human central nervous system. Neuron 2018;97:1284–1298.e7. https://doi.org/10.1016/j.neuron.2018.02.015.
[28] Iwata M, Watanabe S, Yamane A, Miyasaka T, Misonou H. Regulatory mechanisms for the axonal localization of tau protein in neurons. Mol Biol Cell 2019;30:2441–57. https://doi.org/10.1091/mbc.E19-03-0183.
[29] Zempel H, Dennissen FJA, Kumar Y, Luedtke J, Biernat J, Mandelkow EM, et al. Axodendritic sorting and pathological missorting of Tau are isoform-specific and determined by axon initial segment architecture. J Biol Chem 2017;292(29):12192–207. https://doi.org/10.1074/jbc.M117.784702.
[30] Chang CW, Evans MD, Yu X, Yu GQ, Mucke L. Tau reduction affects excitatory and inhibitory neurons differently, reduces excitation/inhibition ratios, and counteracts network hypersynchrony. Cell Rep 2021;37:109855. https://doi.org/10.1016/j.celrep.2021.109855.
[31] Miyamoto T, Stein L, Thomas R, Djukic B, Taneja P, Knox J, et al. Phosphorylation of tau at Y18, but not tau-fyn binding, is required for tau to modulate NMDA receptor-dependent excitotoxicity in primary neuronal culture. Mol Neurodegener 2017;12:1–19. https://doi.org/10.1186/s13024-017-0176-x.
[32] Amadoro G, Ciotti MT, Costanzi M, Cestari V, Calissano P, Canu N. NMDA receptor mediates tau-induced neurotoxicity by calpain and ERK/MAPK activation. Proc Natl Acad Sci U S A 2006;103:2892–7. https://doi.org/10.1073/pnas.0511065103.
[33] Nygaard TG, Duvoisin RC, Manocha M, Chokroverty S. Seizures in progressive supranuclear palsy. Neurology 1989;39:138–40. https://doi.org/10.1212/WNL.39.1.138.
[34] Sánchez MP, García-Cabrero AM, Sánchez-Elexpuru G, Burgos DF, Serratosa JM. Tau-induced pathology in epilepsy and dementia: notions from patients and animal models. Int J Mol Sci 2018;19(4):1092. https://doi.org/10.3390/IJMS19041092.
[35] Lopez A, Lee SE, Wojta K, Ramos EM, Klein E, Chen J, et al. A152T tau allele causes neurodegeneration that can be ameliorated in a zebrafish model by autophagy induction. Brain 2017;140:1128. https://doi.org/10.1093/BRAIN/AWX005.
[36] Decker JM, Krüger L, Sydow A, Dennissen FJ, Siskova Z, Mandelkow E, et al. The Tau/A152T mutation, a risk factor for frontotemporal-spectrum disorders, leads to NR2B receptor-mediated excitotoxicity. EMBO Rep 2016;17(4):552–69. https://doi.org/10.15252/embr.201541439.
[37] Carlomagno Y, Chung DEC, Yue M, Kurti A, Avendano NM, Castanedes-Casey M, et al. Enhanced phosphorylation of T153 in soluble tau is a defining biochemical feature of the A152T tau risk variant. Acta Neuropathol Commun 2019;7:10. https://doi.org/10.1186/S40478-019-0661-2.
[38] Choudhary B, Mandelkow E, Mandelkow EM, Pir GJ. Glutamatergic nervous system degeneration in a C. elegans TauA152T tauopathy model involves pathways of excitotoxicity and Ca2+ dysregulation. Neurobiol Dis 2018;117:189–202. https://doi.org/10.1016/J.NBD.2018.06.005.
[39] Pir GJ, Choudhary B, Mandelkow E, Mandelkow EM. Tau mutant A152T, a risk factor for FTD/PSP, induces neuronal dysfunction and reduced lifespan independently of aggregation in a C. elegans Tauopathy model. Mol Neurodegener 2016;11:1–21. https://doi.org/10.1186/s13024-016-0096-1.
[40] Bargmann CI. Neurobiology of the Caenorhabditis elegans genome. Science 1998;282:2028–33. https://doi.org/10.1126/science.282.5396.2028.
[41] Jankowsky JL, Zheng H. Practical considerations for choosing a mouse model of Alzheimer's disease. Mol Neurodegener 2017;12(1):89. https://doi.org/10.1186/S13024-017-0231-7.
[42] Rudy CC, Hunsberger HC, Weitzner DS, Reed MN. The role of the tripartite glutamatergic synapse in the pathophysiology of Alzheimer's disease. Aging Dis 2015;6:131–48. https://doi.org/10.14336/AD.2014.0423.
[43] Liu G, Fiock KL, Levites Y, Golde TE, Hefti MM, Lee G. Fyn depletion ameliorates tauP301L-induced neuropathology. Acta Neuropathol Commun 2020;8(1):108. https://doi.org/10.1186/S40478-020-00979-6.
[44] Martínez-Mármol R, Small C, Jiang A, Palliyaguru T, Wallis TP, Gormal RS, et al. Fyn nanoclustering requires switching to an open conformation and is enhanced by FTLD-Tau biomolecular condensates. Mol Psychiatry 2023;28(2):946–62. https://doi.org/10.1038/s41380-022-01825-y.
[45] Tracy TE, Madero-Pérez J, Swaney DL, Chang TS, Moritz M, Konrad C, et al. Tau interactome maps synaptic and mitochondrial processes associated with neurodegeneration. Cell 2022;185:712–728.e14. https://doi.org/10.1016/j.cell.2021.12.041.
[46] Mertens J, Herdy JR, Traxler L, Schafer ST, Schlachetzki JCM, Böhnke L, et al. Age-dependent instability of mature neuronal fate in induced neurons from Alzheimer's patients. Cell Stem Cell 2021;28:1533–1548.e6. https://doi.org/10.1016/j.stem.2021.04.004.
[47] Arendt T. Cell cycle activation and aneuploid neurons in alzheimer's disease. Mol Neurobiol 2012;46(1):125–35. https://doi.org/10.1007/s12035-012-8262-0.
[48] Koffie RM, Hyman BT, Spires-Jones TL. Alzheimer's disease: synapses gone cold. Mol Neurodegener 2011;6(1):63. https://doi.org/10.1186/1750-1326-6-63.
[49] Paonessa F, Evans LD, Solanki R, Larrieu D, Wray S, Hardy J, et al. Microtubules deform the nuclear membrane and disrupt nucleocytoplasmic transport in tau-mediated frontotemporal dementia. Cell Rep 2019;26(3):582–593.e5. https://doi.org/10.1016/j.celrep.2018.12.085.
[50] Conze C, Rierola M, Trushina NI, Peters M, Janning D, Holzer M, et al. Caspase-cleaved tau is senescence-associated and induces a toxic gain of function by putting a brake on axonal transport. Mol Psychiatry 2022;27(7):3010–23. https://doi.org/10.1038/s41380-022-01538-2.

[51] Ng B, Vowles J, Bertherat F, Abey A, Kilfeather P, Beccano-Kelly D, et al. Tau depletion in human neurons mitigates Aβ-driven toxicity. Mol Psychiatry 2024;29(7):2009–20. https://doi.org/10.1038/s41380-024-02463-2.

[52] Kuijlaars J, Oyelami T, Diels A, Rohrbacher J, Versweyveld S, Meneghello G, et al. Sustained synchronized neuronal network activity in a human astrocyte co-culture system. Sci Rep 2016;6:36529. https://doi.org/10.1038/SREP36529.

[53] Izsak J, Seth H, Andersson M, Vizlin-Hodzic D, Theiss S, Hanse E, et al. Robust generation of person-specific, synchronously active neuronal networks using purely isogenic human iPSC-3D neural aggregate cultures. Front Neurosci 2019;13:351. https://doi.org/10.3389/fnins.2019.00351.

[54] Trujillo CA, Gao R, Negraes PD, Gu J, Buchanan J, Preissl S, et al. Complex oscillatory waves emerging from cortical organoids model early human brain network development. Cell Stem Cell 2019;25(4):558–569.e7. https://doi.org/10.1016/J.STEM.2019.08.002.

[55] Zafeiriou MP, Bao G, Hudson J, Halder R, Blenkle A, Schreiber MK, et al. Developmental GABA polarity switch and neuronal plasticity in Bioengineered Neuronal Organoids. Nat Commun 2020;11(1):3791. https://doi.org/10.1038/S41467-020-17521-W.

[56] Marshall GF, Gonzalez-Sulser A, Abbott CM. Modelling epilepsy in the mouse: challenges and solutions. Dis Model Mech 2021;14(3):dmm047449. https://doi.org/10.1242/DMM.047449/237833.